ANL/CHM/CP-100829

(28th Symposium (International) on Combustion, Dec. 15, 1999)

RATE CONSTANTS FOR $H_2CO + O_2 \rightarrow HCO + HO_2$ AT HIGH TEMPERATURE

By

J. V. Michael*, M.-C. Su&, J. W. Sutherland#, D.-C. Fang,

L. B. Harding, and A. F. Wagner

Chemistry Division, Argonne National Laboratory, Argonne, IL 60439, USA

Corresponding Author: **Dr. J. V. Michael**
D-193, Bldg. 200
Argonne National Laboratory
Argonne, IL 60439, USA
Phone: (630) 252-3171, Fax: (630) 252-4470
E-mail: Michael@anlchm.chm.anl.gov

Presentation Mode: Oral Presentation
Preferred Publication: Proceedings
Category: Reaction Kinetics of Combustion

	Text	Reference	Tables	Figures	Total
Count	11 pages	29 citations	2 pages	4 pages	
Equiv. Words	3668	568	400	800	5436

&Faculty Research Participant, Department of Educational Programs, Argonne, permanent address: Department of Chemistry, Butler University, Indianapolis, IN 46208

#Present address: Visiting Scientist, Department of Applied Science, Brookhaven National Laboratory, Upton, NY 11973

This work was supported by the U. S. Department of Energy, Office of Basic Energy Sciences, Division of Chemical Sciences, under Contract No. W-31-109-Eng-38.

DISCLAIMER

Abstract

The reaction between H_2CO and O_2 has been studied in a reflected shock tube apparatus between 1633-2027 K using trioxane, $(H_2CO)_3$, as the source of H_2CO. O-atom atomic resonance absorption spectrometry (ARAS) was used to observe absolute $[O]_t$ under conditions of low $[H_2CO]_0$ so that most secondary reactions were negligible. Hence, the observed $[O]_t$ was the direct result of the rate controlling reaction between H_2CO and O_2. *Ab initio* theoretical results indicated that the process, $H_2CO + O_2 \rightarrow HCO + HO_2$, is the only possible reaction. After rapid HCO and HO_2 dissociations, O-atoms are then instantaneously produced from $H + O_2 \rightarrow O + OH$. Using the *ab initio* result, variational transition state theoretical calculations (CTST) give $k_1 = 4.4929 \times 10^{-20} T^{2.9116} \exp(-18692/T)$ cm^3 $molecule^{-1}$ s^{-1}. This theoretical result is consistent with the present experimental determinations and those at lower temperatures.

Introduction

The reaction,

$$H_2CO + O_2 \rightarrow HCO + HO_2, \qquad (1)$$

was originally proposed by Baldwin et al. [1,2] to explain low temperature, 713-816 K, formaldehyde oxidation experiments. Over this relatively small temperature range, their results followed the Arrhenius expression,

$$k_1 = 3.39 \times 10^{-11} \exp(-19576\ K/T)\ cm^3\ molecule^{-1}\ s^{-1}. \qquad (2)$$

This expression was accepted by Tsang and Hampson [3] but was modified to,

$$k_1 = 1 \times 10^{-10} \exp(-20460\ K/T)\ cm^3\ molecule^{-1}\ s^{-1}, \qquad (3)$$

by Baulch et al. [4]. The methane oxidation mechanisms from Leeds [5] and GRI-Mech [6] have adopted Eq. (3) as the rate constant for the title reaction.

In a recent study from this laboratory on the reaction, $CH_3 + O_2 \rightarrow CH_3O + O$ [7], absolute O-atom concentration profiles were determined between 1600-2100 K under very low $[CH_3]_0$. These experiments were designed so that $[O]_t$ against t in the initial stages of reaction would almost exclusively reflect the rate of the methyl with oxygen reaction; i. e., the experiments effectively isolated the reaction. However, it was found for higher temperature experiments that additional [O] was produced from other reactions that had to involve H_2CO in some way. In order to explain these earlier results, the title reaction had to be included with a rate constant ~3-5 times greater than Eqs. (2) or (3). With several

assumptions about the potential energy surface, subsequent conventional transition state theoretical calculations (CTST) were presented [7] that could agree with the higher estimates, but it was further suggested that experimental confirmation of this higher rate would definitely be necessary. This supplies the motivation for the present study.

Using O-atom atomic resonance absorption spectrometry (ARAS), we have directly studied reaction (1) under experimental conditions that are almost exactly the same as the earlier $CH_3 + O_2$ study [7]; i. e., under low $[H_2CO]_0$, We have applied modern *ab initio* electronic structure calculations to determine the potential energy of interaction, and this information has then been used to estimate the thermal rate behavior for reaction (1) using variational transition state theory. This theoretical calculation is then compared to the experimental results.

Experimental

The present experiments were performed with previously described equipment [8] and, therefore, only a brief description of the system, along with those features unique to the current experimental procedures, will be presented here.

The apparatus consists of a 7-m (4 in. o.d.) 304 stainless steel tube separated from the He driver chamber by a 4 mil unscored 1100-H18 aluminum diaphragm. The tube was routinely pumped between experiments to less than 10^{-8} Torr by an Edwards Vacuum Products Model CR100P packaged pumping system. The velocity of the shock wave was measured with eight equally spaced pressure transducers (PCB Piezotronics, Inc., Model 113A21) mounted along the downstream part of the test section of the shock tube and recorded with a 4094C Nicolet digital oscilloscope. Temperature and density in the reflected shock wave regime were calculated from this velocity. This procedure has been given previously, and corrections for boundary layer perturbations have been applied [8,9]. The digital oscilloscope was triggered by pulses derived from the last velocity gauge signal. The photometer system was radially located 6 cm from the endplate. All optics were made

from MgF_2. The resonance lamp beam intensity was measured by an EMR G14 solar blind photomultiplier tube and recorded with the oscilloscope.

The ARAS technique has been used for the detection of the transient O-atoms. In earlier work [10], an O-atom curve-of-growth was determined using $X_{O_2} = 1 \times 10^{-3}$ in 1.8 Torr of purified grade He at 50 watts microwave power to give an effective lamp temperature of 490 K [11]. This curve-of-growth was subsequently used and slightly modified in the later work [7]. The present work was carried out in exactly the same way as this earlier study except that H_2CO was used as the reactant instead of CH_3. Following procedures discussed earlier [7], twenty-four kinetics experiments were carried out between 1633 and 2027 K under the conditions shown in Table 1.

Gases: High purity He (99.995%), used as the driver gas, was from Air Products and Chemicals, Inc. Scientific grade Kr (99.999%) and ultra-high purity He (99.999%), the diluent gases in reactant mixtures, were from Spectra Gases, Inc. and AGA Gases, respectively. In Kr, the ~10 ppm impurities (N_2 - 2 ppm, O_2 - 0.5 ppm, Ar - 2 ppm, CO_2 - 0.5 ppm, H_2 - 0.5 ppm, CH_4 - 0.5 ppm, H_2O - 0.5 ppm, Xe - 5 ppm, and CF_4 - 0.5 ppm) are all either inert or in sufficiently low concentration so as to not perturb O-atom profiles. The ultra-high purity grade He was also used for the resonance lamp. High purity O_2 (99.995%) for the atomic filter was from AGA Gases. Scientific grade O_2 (99.999%), for reaction mixtures, was obtained from MG Industries. As an H_2CO source, 99% 1,3,5 trioxane, $(H_2CO)_3$, from Aldrich Chemical Co. was subjected to bulb-to-bulb distillation retaining the middle third. The thoroughly outgassed product had sufficient vapor pressure for accurate mixture preparation. On shock heating, three molecules of H_2CO were instantaneously formed from the fast thermal decomposition of $(H_2CO)_3$ as described in previous reports [12,13]. Test gas mixtures were accurately prepared from pressure measurements using a Baratron capacitance manometer and were stored in an all glass vacuum line.

Results

With the relatively high levels of O_2 used in this work, there is slight resonance light absorption at 130 nm by O_2. This absorption is uniform over the O_2 bandwidth and $[O_2]$ does not change appreciably during an experiment. Therefore, any observed absorbance increase without reactant reflects both a total density increase due to vibrational relaxation of O_2 at low temperature and/or O-atom formation from $O_2 + M \rightarrow 2O + M$ at high temperature. Therefore, with the same $[O_2]$ as used in the kinetics experiments, a limited set of O_2 dissociation experiments were performed. Under conditions where O-atom formation was negligible, density relaxation (generally <250 μs at T > 1600 K) was easily determined. The apparent absorbance relaxation due to 130 nm absorption by O_2 was then point-by-point subtracted from the higher temperature runs where O-atoms were definitely formed from dissociation. The corrected absorbance was then converted to $[O]_t$ with the previously determined curve-of-growth [7]. Using the expression, $k_d = R_O/2[O_2][Kr]$, where R_O is the rate of formation of O-atoms (i. e., the slope from the experimental $[O]_t$ against t plots), values for k_d were determined. For T > 2200 K the results were within ±40% of those already accurately determined by Jerig, Thielen, and Roth [14]. Hence, we have adopted their value in the kinetics model for the H_2CO/O_2 experiments. It should be noted that O-atom production rates from decomposition starts to dominate above ~2100 K, and, therefore, we have excluded all experiments above 2027 K. In the Table 1 kinetics runs, we also corrected for O_2 density relaxation by point-by-point subtraction. Realizing that He would be a better relaxation collider than Kr, a set of experiments were also carried out with mixtures containing ~6% He in order to investigate whether O_2 vibrational relaxation could effect the observed rate constants. Experiments with no added H_2CO were also performed for use as blank subtractions from the subsequent kinetics runs. For both the experiments with and without added He, the contribution of the correction was ~20%; i. e., 80% of the signal was due to chemical reaction with reactant H_2CO. Using the curve-of-growth [7],

absorbance was converted to $[O]_t$ giving profiles like that shown in Fig. 1. To understand this result and those from the other experiments of Table 1, it is necessary to numerically integrate an appropriate chemical mechanism, included in Table 2, to predict O-atom profiles. It should be noted that the mechanism does not have to be inclusive since the secondary chemistry cannot be highly perturbing because $[H_2CO]_0$ is so low.

Discussion

The profile in Fig. 1 at T = 1802 K was obtained with $[H_2CO]_0 = 4.06 \times 10^{12}$ molecule cm^{-3}, and, within 800 μs, [O] reaches a value approximately equal to $[H_2CO]_0$. In 800 μs at 1802 K, destruction of H_2CO by two thermal decomposition channels [13] is only ~0.1 $[H_2CO]_0$, indicating unambiguously that a direct bimolecular reaction between H_2CO and O_2 is the only possible source for the production of the observed $[O]_t$. As discussed earlier [7] and in more detail below, the most probable products from such a reaction are HCO + HO_2; i. e., reaction (1). At T>1600 K, both HCO and HO_2 will decompose, effectively instantaneously on the time scale of these experiments, giving 2H + CO + O_2. With the large $[O_2]$ present, the two H-atoms will instantaneously be converted to O + OH, through the reaction, H + O_2 → O + OH, giving rise to the observed [O]. Neglecting the small contribution from H_2CO thermal decomposition, the initial rate of formation of O-atoms, R_O, is then ~$2k_1[H_2CO]_0[O_2]_0$. However, depending on temperature and initial reactant concentrations, H_2CO decomposition might compete and secondary reactions might slightly perturb measured $[O]_t$. Hence, we have used the fourteen-step mechanism of Table 2 to simulate the experimental results. Rate constants for all reactions in the table are accurately known with the title reaction being the only unknown quantity to be fitted. Note that the subsequent reactions of O and H with H_2O are not included because these reactions are too slow under the present conditions.

Figure 1 shows a simulation with $k_1 = 5 \times 10^{-15}$ cm^3 $molecule^{-1}$ s^{-1}. Absolute [O] is known to only ±10% from the curve-of-growth [7], and the simulation, in comparison to

experiment, is roughly within this range. Simulations were also carried out with k_1 doubled and halved resulting in predicted values ~0.55 and ~1.7 times $[O]_t$ (obtained with 5 x 10^{-15} cm^3 $molecule^{-1}$ s^{-1}), respectively, indicating major sensitivity to the fitted k_1. k_1 could be determined to within ~±20%; i. e., the fit can be considered to give k_1 under almost chemical isolation conditions. To further illustrate this point, we performed simulations that included only reactions (1), (4), (5), and (7) (i. e., with all other rate constants taken to be zero including the thermal decomposition channels for H_2CO), and the simulation was only ~5% higher than that shown in Fig. 1. This is well within experimental error.

Figure 2 shows two more experiments and mechanism simulations using Table 2, at respective temperatures, 2027 and 1690 K. Using only reactions (1), (4), (5), and (7) at 2027 K, predicted $[O]_t$ is ~5-20% higher than shown; however, this increase is caused by H_2CO thermal decomposition because including reactions (2) and (3) in Table 2 brings the values to within ±3% of the full simulation. With larger $[H_2CO]_0$, the simulation at 1690 K, using reactions (1), (4), (5), and (7), gives values that are in sufficient agreement with the full simulation for ~500 μs. However, at longer times the calculations diverge with the reduced mechanism predicting only 0.63 of the value obtained with the full mechanism at 1400 μs. This obviously means that secondary reactions become relatively more important at longer times with larger $[H_2CO]_0$. The initial time behavior for both experiments is however strongly sensitive to the fitted k_1, and changes of ±20% result in worse fits.

The other twenty-one experiments in Table 1 were then simulated in exactly the same way as the three experiments of Figs. 1 and 2. The fitted values of k_1 are listed in Table 1 and are plotted in Arrhenius form in Fig. 3. The scatter in values over the quite low range in T^{-1} precludes determining an Arrhenius expression for the rate behavior; however, the present results can be compared to the Baulch et al. [4] recommendation, Eq. (3). The line shown in Fig. 3 is calculated from Eq, (3) and is seen to be in excellent agreement up to $T \cong 1800$ K. However, at 2050 K, Eq. (3) gives ~20-30% of the experimental value.

In earlier work from this laboratory on the $CH_3 + O_2$ reaction [7], k_1 values were derived on the assumption that the longer time $[O]_t$ behavior at high temperature was due to reaction (1). Figure 4 shows a comparison between those earlier inferences (open circles) and the present direct data (closed circles). Since the values above ~1800 K agree remarkably well, the earlier inference is corroborated. However, between 1600-1800 K there is about a factor of two to three discrepancy between the present and earlier values that may be due to the assumption of complete and instantaneous trioxane decomposition. The question can then be asked as to what effect this discrepancy might have on the reported rate constants for the $CH_3 + O_2 \rightarrow CH_3O + O$ reaction. Since these rate constants were primarily based on initial rates, the effects of reaction (1) would be quite minimal. Any adjustment would not appreciably change the reported values outside the experimental error associated with those data. Figure 4 also shows the range of values found by Walker and coworkers (Eqn. (2) and solid squares) [1,2] along with the Baulch et al. recommendation (Eqn. (3) and solid line) [4]. Both appear to underestimate the rate constants for reaction (1) at high temperatures.

Theory: In the earlier work [7], simple theoretical models were used to justify the importance of reaction (1). Using modern electronic structure calculations of the potential energy of interaction followed by subsequent calculations of thermal rate constants, this issue is considerably expanded in the present work.

The electronic structure methodology is coupled cluster, CCSD(T), employing the Dunning [21] correlation-consistent polarized valence double zeta basis set (cc-pvdz). The CCSD(T) method is generally regarded as the most accurate, single-reference, *ab initio* method currently available. All calculations were carried out using the MOLPRO package of codes [22-25].

The predicted CCSD(T)/cc-pvdz, transition state properties are as follows: R_{CO} = 1.19Å, R_{CHa} = 1.14Å, R_{CHb} = 1.45Å, R_{Ohb} = 1.14Å, R_{OO} = 1.30Å, $H_aCO\angle$ = 127° , $H_bCO\angle$ = 135°, $CH_bO\angle$ = 150°, and $H_bOO\angle$ = 104°. The structure is planar with both the OHCH

and CHOO dihedral angles in cis orientations. As expected for an endothermic reaction the transition state is "late" with an OH bond extension of 0.16Å, relative to HO_2, and a CH bond extension of 0.32Å, relative to H_2CO. The calculated harmonic frequencies for this transition state are: in-plane; 2754, 1915, 1692, 1262, 1134, 606, 330, 163, and 2034i cm^{-1}, and out-of-plane; 1059, 406, and 112 cm^{-1}. These can be compared to calculated frequencies for HCO of 2646, 1884 and 1116 cm^{-1} and, for HO_2, of 3650, 1427, 1101 cm^{-1}. The calculations predict that this transition state does not lead directly to HO_2 + HCO but rather to a long-range complex between HO_2 and HCO, which is predicted to be a bound species 5.3 kcal $mole^{-1}$ below HO_2 + HCO. The existence of this long-range complex results in both a lower and more centrally located barrier.

The calculations predict an overall endothermicity for the reaction of 41.6 kcal $mole^{-1}$ (including zero point corrections). This can be compared with the experimental result of 39.0 ± 0.8 kcal/mole (obtained by taking the difference between the CH bond energy of H_2CO, 86.57 ± 0.16 kcal $mole^{-1}$ [26] and the OH bond energy of HO_2, 47.6 ± 0.8 kcal $mole^{-1}$ [27]). For the reaction $H_2 + O_2 \rightarrow HO_2 + H$, it was found [20] that using a larger basis set, cc-pvqz instead of cc-pvdz, decreases the endothermicity by 2.3 kcal $mole^{-1}$, yielding a result in excellent agreement with experiment. A 2.3 kcal $mole^{-1}$ decrease in the calculated endothermicity of reaction (1) would also lead to near perfect agreement between theory and experiment. Unfortunately it was not possible to do cc-pvqz calculations on reaction (1). However, the previous calculations [20] also showed that the barrier height in the exothermic direction is much less sensitive to basis set than the barrier in the forward direction, changing by only 0.2 kcal $mole^{-1}$ on going from the cc-pvdz basis set to the cc-pvqz. The calculated, cc-pvdz, barrier (including zero point corrections) for reaction (-1) is -0.9 kcal $mole^{-1}$, relative to HCO + HO_2 or +2.8 kcal $mole^{-1}$ relative to the complex. This is the result that will be used in the rate constant calculations to follow.

The first calculations are conventional transition state theory using only the properties of the transition state discussed above. If all the degrees of freedom

perpendicular to the reaction path are treated harmonically, then the dotted line of Fig. 4 is obtained. The rate that is directly calculated is in the reverse HO_2 + HCO direction. The experimental equilibrium constant with the latest experimental value for the heat of reaction [27] is then used to get the forward rate constant. This approach corrects for the slightly different heat of reaction in the calculations discussed above. The approach is used for all the calculated rates discussed below.

In order to examine variational effects on this harmonic rate constant, an approximate reaction path was created by modifying a density-functional-theory (DFT)/cc-pvdz reaction path so as to reproduce the CCSD(T) energies at the CCSD geometries for the transition state and complex. (Although relatively inexpensive, the DFT calculation by itself is significantly in error, with a barrier more than 4 kcal $mole^{-1}$ lower than the CCSD value.) With this approximate reaction path, the transition state was found to be localized at all temperatures at the top of the barrier indicating that conventional transition state theory is adequate.

As seen in Fig. 4, the harmonic rate constant is significantly lower than all measurements. However, because of the low frequencies at the transition state, one or more of the perpendicular degrees of freedom should perhaps be treated as free or hindered rotors. Of the lowest four frequencies, the first and the last involve out-of-plane motion while the middle two are for in-plane motion. Any in-plane internal rotational motion must inevitably rotate the two reactants away from their optimal orientation for forming the incipient H---C bond and expose the non-reactive portions of the reactants to each other. Thus such internal rotations could be expected to have high barriers. However, there are two out-of-plane internal rotations that could be performed without influencing the favorable orientation of the bond, namely internal rotation about the incipient H---C bond axis and internal rotation about the weakened H---O bond axis. Barriers in this case would not involve a degradation in the bonding but rather an increase in repulsion as the rotating fragments move past each other.

To investigate the barriers for such motion, CCSD/cc-pvdz calculations were performed for the full range of rotational angles both for the HCO rotation about the incipient H---C bond axis and for the radical O rotation about the weakened H---O bond axis. The results indicate in both cases a maximum barrier at the planar geometry with the rotating reactant flipped by 180° from the transition state geometry. The respective barriers are 6.2 and 4.7 kcal $mole^{-1}$ for HCO and HOO rotations, respectively. While these are substantial barriers at low temperatures, at the temperatures of Table 1, such barriers are relatively easily surmounted. These barriers and the reduced moments of inertia for counter rotating fragments about the two axes are what is required to compute a hindered rotation partition function using the approach of Pitzer and Gwinn [28]. Incorporation of these partition functions in replacement of the two vibrational partition functions for the lower frequency out-of-plane vibrations leads to the bold solid line in Fig. 4.

The hindered rotor calculated rate constant is very much larger than the harmonic oscillator calculated rate constant at all temperatures, but especially so at the higher temperatures for the measurements in Table 1. Comparison to a free rotor version shows that at the high temperatures of these measurements, the hindered rotations are about 30% free. The hindered rotor rate constants roughly support the measurements of Table 1, are consistent with the inferred values from ref. 7, and are in agreement with the more indirect measurements of Baldwin et al. They definitely suggest greater rate constant curvature than shown by the Baulch et al. [4] recommendation.

There are two final comments concerning the computed rate constants. First, the large variation between the harmonic and hindered rotor rates suggests that a more complete hindered rotor treatment including the other low frequency modes and the external rotation is probably necessary to calculate the rate constant with precision. Within the classical approximation of Flexible Transition State Theory with variable reaction coordinate [29], such a rate constant calculation can be carried out if the fully dimensional hindered rotor potential is know. Such calculations are beyond the scope of this work and the calculated

results in Fig. 4 will not be refined further. Second, directly calculating the reverse reaction of HO_2 + HCO with hindered rotations might seem to lead to complications from other reactive channels that lead to products HOOH + CO or HOOCHO. Perhaps hindered rotations will sample these two reaction paths. Fortunately, while both of these reactions are possible, they occur on a singlet surface, not the triplet surface being considered here.

In conclusion, the experimental and theoretical results both indicate that the rate constant for reaction (1) used in modeling codes [5,6] are substantially underestimated at high temperature. The present theoretical results can be expressed by the three parameter expression:

$$k_1 = 4.4929 \times 10^{-20}\, T^{2.9116} \exp(-18692/T)\ cm^3\ molecule^{-1}\ s^{-1} \qquad (4)$$

to within ±6% for 500-3000 K. The experimental to theoretical agreement is only adequate due to the great complexity of the interaction as evidenced by the *ab initio* results, Even so, we suggest that Eqn. (4) is clearly a better choice for use in chemical modeling at higher temperatures than either the Walker and coworkers result, Eqn. (2), or the Baulch et al. result, Eqn. (3).

Acknowledgments: This work was supported by the U. S. Department of Energy, Office of Basic Energy Sciences, Division of Chemical Sciences, under Contract No. W-31-109-Eng-38.

References

1. Baldwin, R. R., Langford, D., Matchan, M. J., Walker, R. W. and Yorke, D. A., *Thirteenth Symposium (International) on Combustion*; The Combustion Institute: Pittsburgh, PA, 1971; p. 251.
2. Baldwin, R. R., Fuller, A. R., Longthorn, D. and Walker, R. W., *J. Chem. Soc. Faraday Trans. 1* 70:1257-1268 (1974).
3. Tsang, W. and Hampson, R. F., *J. Phys. Chem. Ref. Data* 15:1087-1279 (1986).

4. Baulch, D. L., Cobos, C. J., Cox, R. A., Esser, C., Frank, P., Just, Th., Kerr, J. A., Pilling, M. J., Troe, J., Walker, R. W. and Warnatz, J., *J. Phys. Chem. Ref. Data* 21:411-429 (1992).
5. Pilling, M. J., Turanyi, T., Hughes, K. J. and Clague, A. R., *The Leeds methane oxidation mechanism 1.3*, http://www.chem.leeds.ac.uk/Combustion/Combustion.html.
6. Bowman, C. T., Hanson, R. K., Davidson, D. F., Gardiner, Jr., W. C., Lissianski, V., Smith, G. P., Golden, D. M., Frenklach, M. and Goldenberg, M., *GRI-Mech 2.11*, http://www.me.berkeley.edu/gri_mech/.
7. Michael, J. V., Kumaran, S. S. and Su, M.-C., *J. Phys. Chem.* 103:5942-5948 (1999).
8. Michael, J. V., *J. Chem. Phys.* 90:189-198 (1989).
9. Michael, J. V. and Sutherland, J. W., *Int. J. Chem. Kinet.* 18:409-436 (1986).
10. Michael, J. V. and Lim, K. P., *J. Chem. Phys.* 97:3228-3234 (1992).
11. Maki, R. G.; Michael, J. V. and Sutherland, J. W., *J. Phys. Chem.* 89:4815-4821 (1985).
12. Irdam, E. A., Kiefer, J. H., Harding, L. B. and Wagner, A. F., *Int. J. Chem. Kinet.* 25:285-303 (1993).
13. Kumaran, S. S., Carroll, J. J. and Michael, J. V., *Twenty-Seventh Symposium (International) on Combustion*; The Combustion Institute: Pittsburgh, PA, 1998; p. 125.
14. Jerig, L., Thielen, K. and Roth, P., *AIAA J.* 29:1136-1139 (1991).
15. Michael, J. V., *Prog. Energy Combust. Sci.*18:327-347 (1992).
16. Timonen, R. S., Ratajczak, E., Gutman, D. and Wagner, A. F., *J. Phys. Chem.* 91:5325-5332 (1987).
17. Timonen, R. S., Ratajczak, E. and Gutman, D., *J. Phys. Chem.* 92:651-655 (1988).
18. Du, H. and Hessler, J. P., *J. Chem. Phys.* 96:1077-1092 (1992).
19. Michael, J. V., Kumaran, S. S., Su, M.-C. and Lim, K. P., *Chem. Phys. Lett.*, in press.
20. Michael, J. V., Sutherland, J. W., Harding, L. B. and A. F. Wagner, *Proceeding of the Combustion Institute* 28, submitted.
21. Dunning, T. H., Jr., *J. Chem. Phys.* 90:1007-1023 (1989).
22. Hampel, C., Peterson, K. and Werner, H.-J., *Chem. Phys. Lett.* 190:1-12 (1992) and references therein.
23. Werner, H.-J. and Knowles, P. J., *J. Chem. Phys.* 82:5053-5063 (1985)
24. Knowles, P. J. and Werner, H.-J., *Chem. Phys. Lett.* 115:259-267 (1985)

25. Werner, H.-J. and Knowles, P. J., with contributions from Almlof, J., Amos, R. D., Berning, A., Cooper, D. L., Deegan, M. J. O., Dobbyn, A. J., Eckert, F., Elbert, S. T., Hampel, C., Lindh, R., Lloyd, A. W., Meyer, W., Nicklass, A., Peterson, K., Pitzer, R., Stone, A. J., Taylor, P. R., Mura, M. E., Pulay, P., Schutz, M., Stoll, H. and Thorsteinsson, T., MOLPRO, http://www.tc.bham.ac.uk/molpro/; MOLPRO is a package of *ab initio* programs.

26. Chuan, M.-C., Foltz, M.F. and Moore, C.B., *J. Chem. Phys.* 87:3855-3864 (1987).

27. Litorja, M. and Ruscic, B., *J. Electron Spectrosc.* 97:131-146 (1998).

28. Pitzer, K. S. and Gwinn, W. D., *J. Chem. Phys.* 10:428-440 (1942); Pitzer, K. S., *J. Chem. Phys.* 14:239-243 (1946).

29. Klippenstein, S. J., Wagner, A. F., Robertson, S. H., Dunbar, R. C., and Wardlaw, D. M., *VARIFLEX-version 1.0*, http://chemistry.anl.gov/variflex. VARIFLEX is a freeware program package for calculating gas phase reaction rates.

Table 1: High Temperature Rate Data for $H_2CO + O_2$

P_1 / Torr	M_s[a]	ρ_5 / (10^{18} cm^{-3})[b]	T_5 / K[b]	k_1 /(cm^3 s^{-1})[c]
	$X_{(H_2CO)_3} = 5.561 \times 10^{-7}$	$X_{O_2} = 5.877 \times 10^{-2}$		
10.94	2.866	2.868	1923	4.0(-15)[d]
10.89	2.905	2.532	1965	6.0(-15)
10.96	2.765	2.432	1802	5.0(-15)
	$X_{(H_2CO)_3} = 1.157 \times 10^{-6}$	$X_{O_2} = 5.932 \times 10^{-2}$		
10.97	2.816	2.460	1875	2.8(-15)
$X_{(H_2CO)_3} = 1.104 \times 10^{-6}$	$X_{O_2} = 6.103 \times 10^{-2}$	$X_{He} = 6.365 \times 10^{-2}$		
10.93	2.885	2.532	1937	1.1(-14)
10.95	2.826	2.491	1866	1.0(-14)
10.91	2.812	2.471	1848	1.0(-14)
10.95	2.879	2.532	1930	1.8(-14)
10.94	2.829	2.491	1869	1.7(-14)
10.94	2.957	2.587	2027	2.5(-14)
	$X_{(H_2CO)_3} = 5.455 \times 10^{-6}$	$X_{O_2} = 6.075 \times 10^{-2}$		
10.97	2.715	2.398	1741	1.5(-15)
10.88	2.769	2.430	1797	1.0(-15)
10.96	2.710	2.391	1734	4.7(-16)
10.96	2.621	2.316	1633	2.3(-16)
10.92	2.736	2.404	1765	6.5(-16)
10.92	2.822	2.481	1861	1.9(-15)
10.95	2.713	2.399	1732	8.6(-16)
10.93	2.671	2.352	1690	5.4(-16)
10.95	2.750	2.422	1782	1.05(-15)
10.93	2.750	2.418	1781	9.2(-16)
10.93	2.780	2.442	1817	1.0(-15)
10.94	2.624	2.314	1636	2.6(-16)
10.97	2.690	2.377	1711	6.3(-16)
10.96	2.667	2.355	1685	7.0(-16)

[a]The error in measuring the Mach number, M_S, is typically 0.5-1.0 % at the one standard deviation level. [b]Quantities with the subscript 5 refer to the thermodynamic state of the gas in the reflected shock region. [c]Fitted rate constants for reaction (1) (see text). [d]Parentheses denotes the power of 10.

Table 2: Mechanism used for fitting [O] profiles from $H_2CO + O_2$. [a]

1.	$H_2CO + O_2 \rightarrow HCO + HO_2$	k_1 = fitted
2.	$H_2CO + Kr \rightarrow HCO + H + Kr$	$k_2 = 1.019 \times 10^{-8} \exp(-38706\ K/T)$ [b]
3.	$H_2CO + Kr \rightarrow H_2 + CO + Kr$	$k_3 = 4.658 \times 10^{-9} \exp(-32110\ K/T)$ [b]
4.	$H + O_2 \rightarrow OH + O$	$k_4 = 1.62 \times 10^{-10} \exp(-7474\ K/T)$ [c]
5.	$HCO + Kr \rightarrow H + CO + Kr$	$k_5 = 3.1 \times 10^{-7}\ T^{-1} \exp(-8555\ K/T)$ [d]
6.	$HCO + O_2 \rightarrow HO_2 + CO$	$k_6 = 1.26 \times 10^{-11} \exp(-204\ K/T)$ [e]
7.	$HO_2 + Kr \rightarrow H + O_2 + Kr$	$k_7 = 2.0 \times 10^{-5}\ T^{-1.18} \exp(-24363\ K/T)$ [f]
8.	$OH + OH \rightarrow O + H_2O$	$k_8 = 7.19 \times 10^{-21}\ T^{2.7} \exp(1251/T)$ [c]
9.	$OH + H_2 \rightarrow H_2O + H$	$k_9 = 3.56 \times 10^{-16}\ T^{1.52} \exp(-1736\ K/T)$ [c]
10.	$OH + O \rightarrow O_2 + H$	$k_{10} = 5.42 \times 10^{-13}\ T^{0.375} \exp(1112\ K/T)$ [c]
11.	$OH + H_2CO \rightarrow HCO + H_2O$	$k_{11} = 5.70 \times 10^{-15}\ T^{1.18} \exp(225\ K/T)$ [g]
12.	$O_2 + Kr \rightarrow O + O + Kr$	$k_{12} = 2.66 \times 10^{-6}\ T^{-1} \exp(-59380\ K/T)$ [h]
13.	$H_2 + Kr \rightarrow H + H + Kr$	$k_{13} = 8.86 \times 10^{-10} \exp(-48321\ K/T)$ [i]
14.	$H_2 + O_2 \rightarrow H + HO_2$	$k_{14} = 1.228 \times 10^{-18}\ T^{2.4328} \exp(-26926\ K/T)$ [j]

[a]All rate constants are in cm^3 $molecule^{-1}$ s^{-1}. [b]Ref. 13. [c]Ref. 15. [d]Ref. 16. [e]Ref. 17. [f]Ref. 3. [g]Ref. 3, 4. [h]Ref. 14. [i]Ref. 18, 19. [j]Ref. 20.

Figure Captions

Fig. 1 Measured O-atom profile. The conditions are: P_1= 10.96 Torr, M_s = 2.765, $X_{(H2CO)3}$ = 5.561 x 10^{-7}, and X_{O2} = 5.877 x 10^{-2} giving T_5 = 1802 K, ρ_5 = 2.432 x 10^{18} molecules cm^{-3}, $[H_2CO]$ = 4.058 x 10^{12} molecules cm^{-3}, and $[O_2]$ = 1.430 x 10^{17} molecules cm^{-3}. The line is a simulation using the mechanism of Table 2 with k_1 = 5 x10^{-15} cm^3 $molecules^{-1}$ s^{-1}.

Fig. 2 Measured O-atom profiles for two typical experiments. The conditions for the left trace are: P_1= 10.94 Torr, M_s = 2.957, $X_{(H2CO)3}$ = 1.104 x 10^{-6}, X_{O2} = 6.103 x 10^{-2}, and X_{He} = 6.365 x 10^{-2} giving T_5 = 2027 K, ρ_5 = 2.587 x 10^{18} molecules cm^{-3}, $[H_2CO]$ = 8.572 x 10^{12} molecules cm^{-3}, and $[O_2]$ = 1.579 x 10^{17} molecules cm^{-3}. For the right trace: P_1= 10.93 Torr, M_s = 2.671, $X_{(H2CO)3}$ = 5.455 x 10^{-6}, and X_{O2} = 6.075 x 10^{-2} giving T_5 = 1690 K, ρ_5 = 2.352 x 10^{18} molecules cm^{-3}, $[H_2CO]$ = 3.850 x 10^{13} molecules cm^{-3}, and $[O_2]$ = 1.429 x 10^{17} molecules cm^{-3}. The solid lines are simulations using the mechanism of Table 2 with k_1(2027 K) = 2.5 x 10^{-14} and k_1(1690 K) = 5.4 x 10^{-16} cm^3 $molecules^{-1}$ s^{-1}.

Fig. 3 Arrhenius plot of the data for k_1 from Table 1. The line is the recommendation from Baulch et al., ref. 4, as given by Eqn. (3).

Fig. 4 Arrhenius plot of the data (●) for k_1 from Table 1 in comparison to values indirectly inferred from Michael et al., ref. 7 (❍) and measured by Walker and coworkers, refs. 1 and 2 (■). The thin line is from Baulch et al., ref. 4, the dashed line is a completely harmonic conventional transition state theory calculation (see text), and the bold line is the hindered rotor conventional transition state theory calculation (see text).

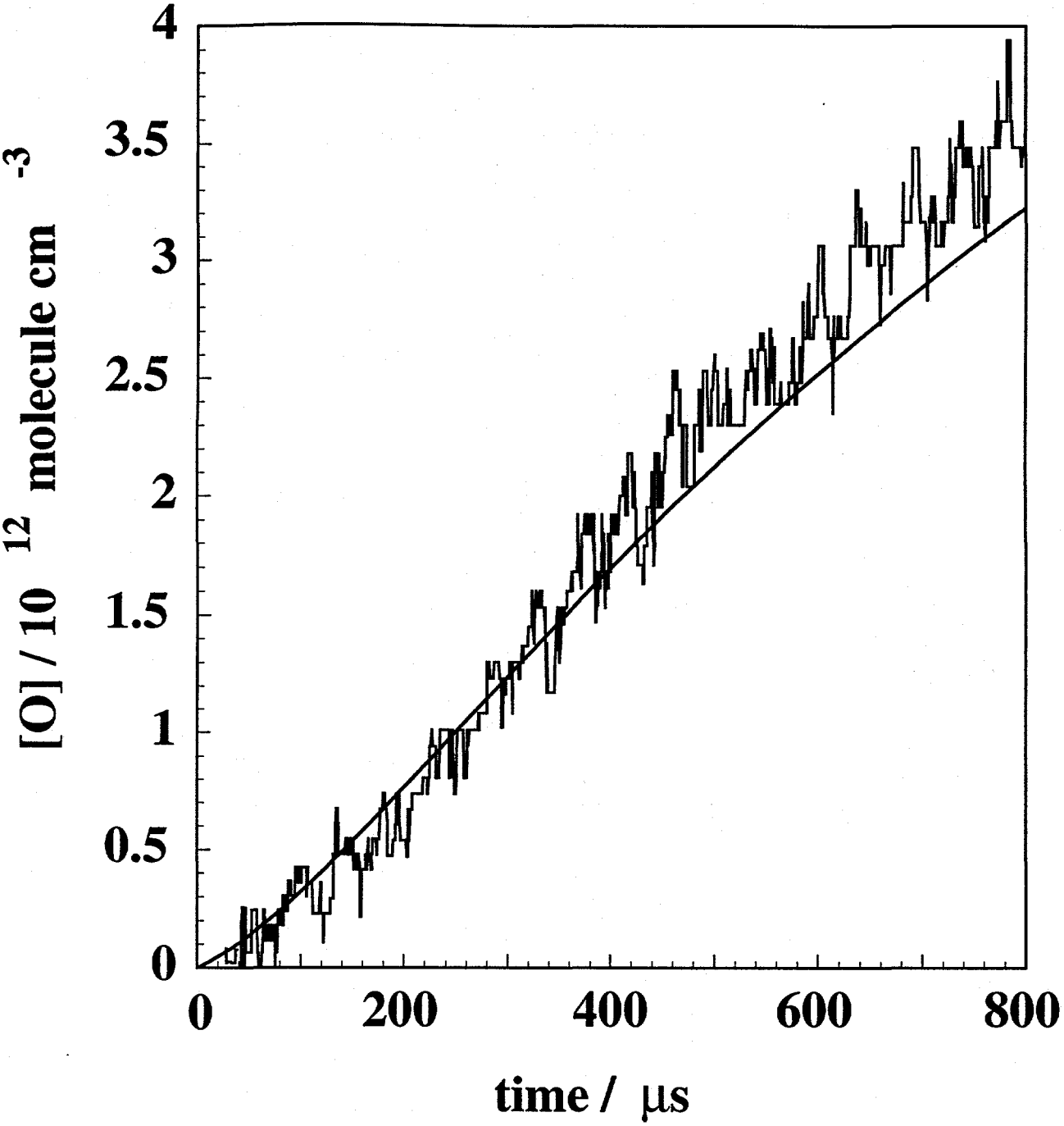

Fig. 1

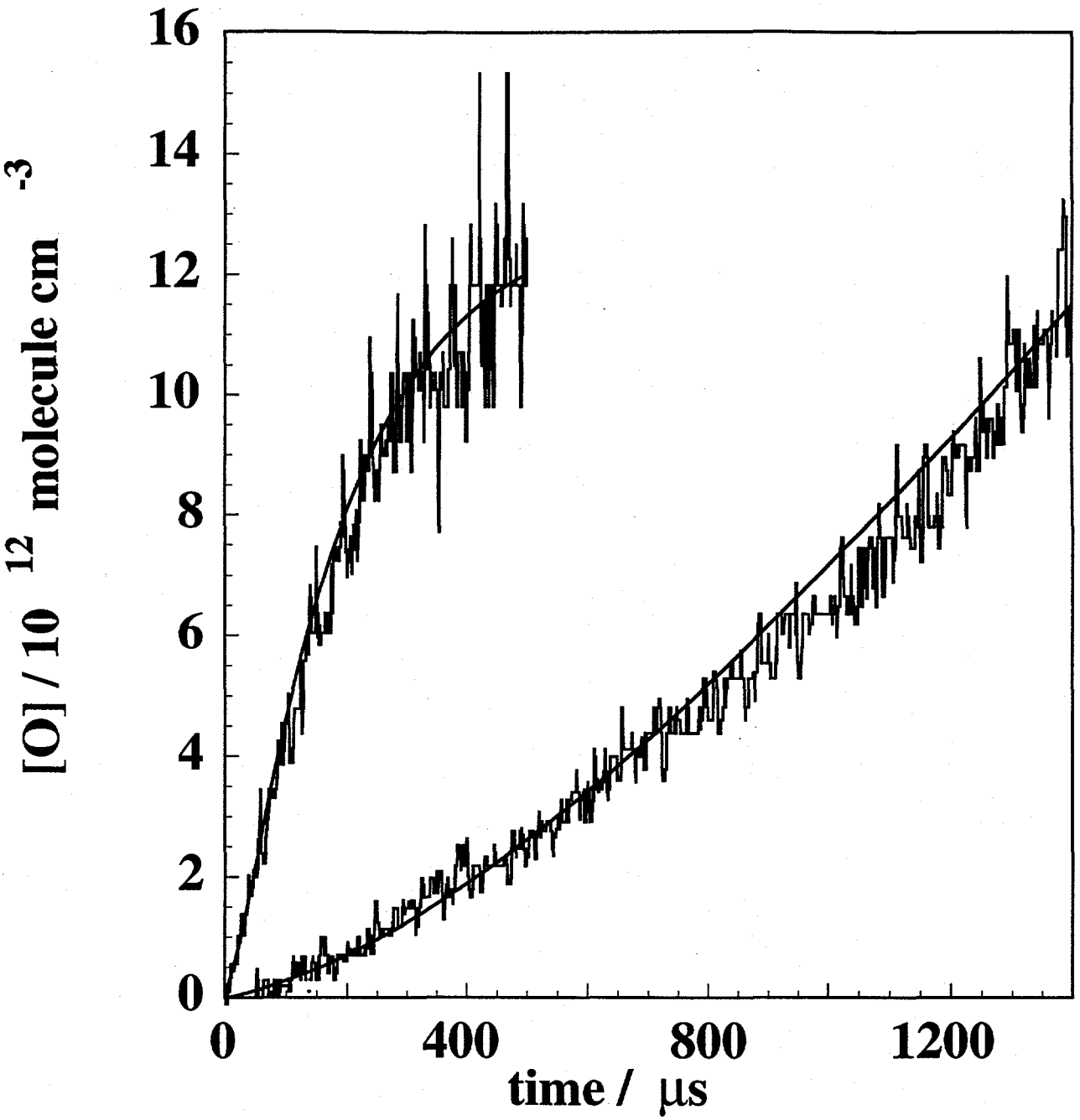

Fig 2

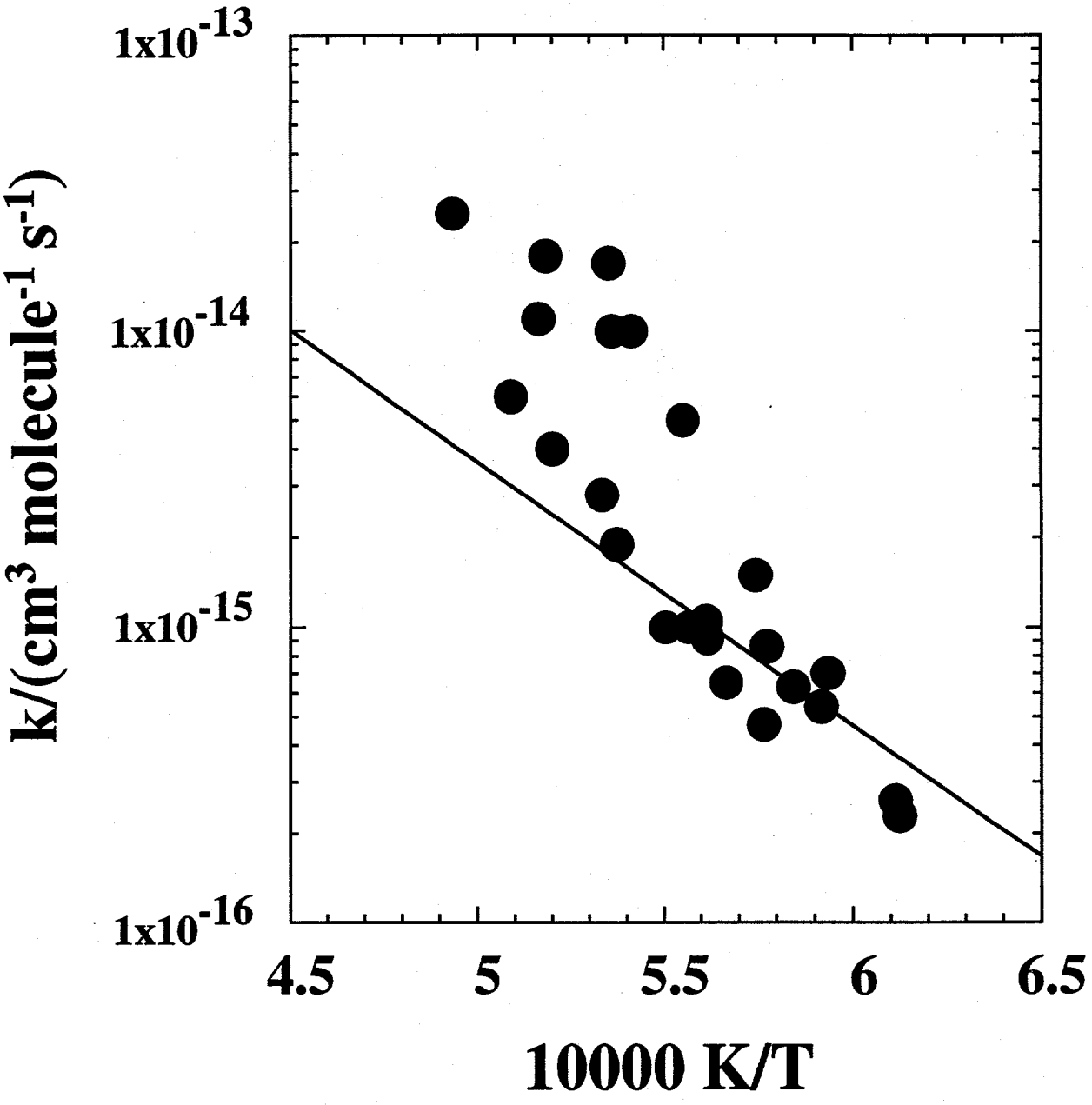
1x10-13
1x10-14
1x10-15
1x10-16
k/(cm3 molecule-1 s-1)
4.5
5
5.5
6
6.5
10000 K/T

Fig 3

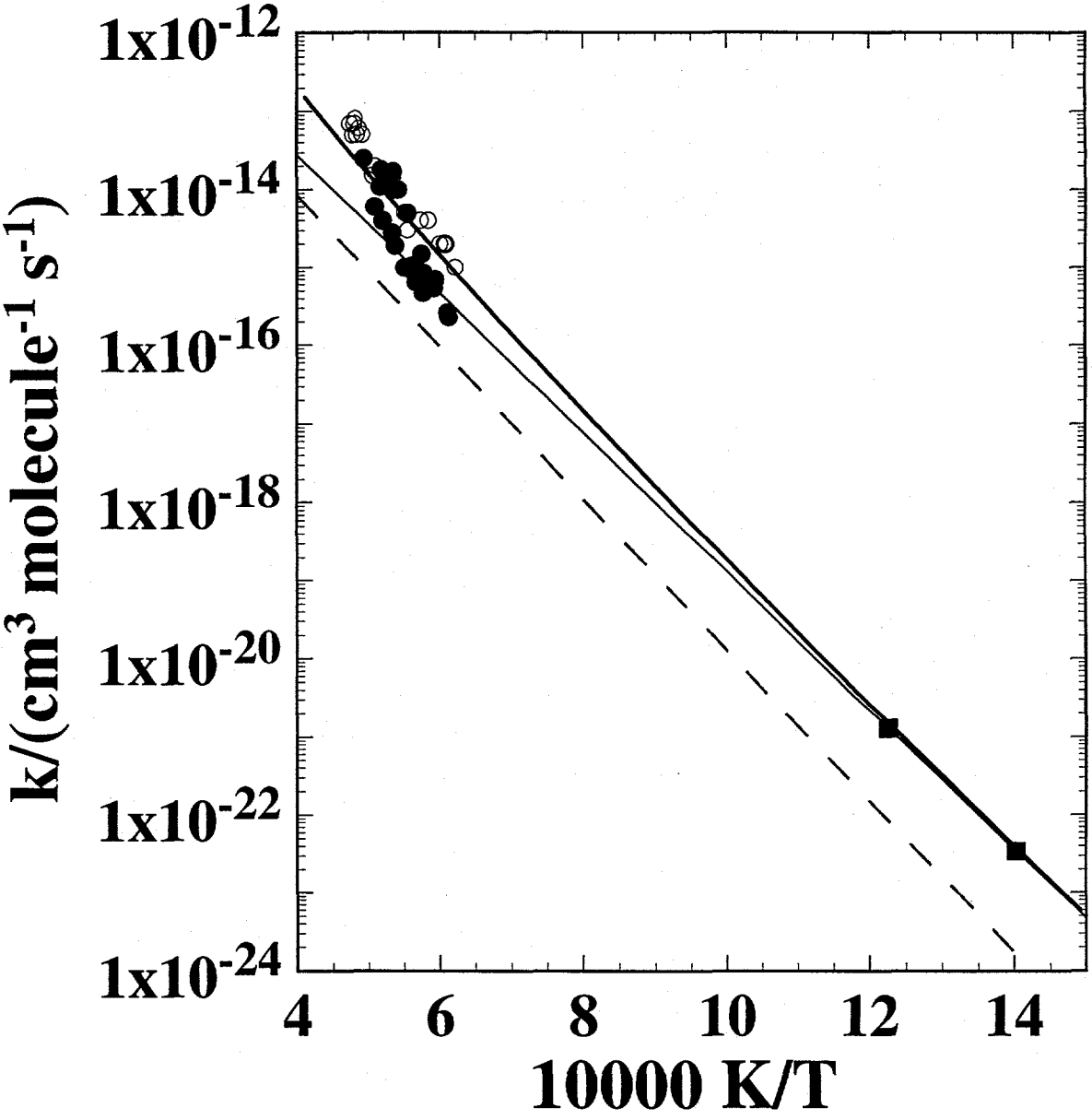
1x10-12
1x10-14
1x10-16
1x10-18
1x10-20
1x10-22
1x10-24
k/(cm3 molecule-1 s-1)
4
6
8
10
12
14
10000 K/T

Fig 5